Luminescence spectroscopy of matrix-isolated atomic manganese: Site size and orbital occupancy dependence of crystal field splitting

Martin A. Collier, Owen Byrne, Ciaran Murray, and John G. McCaffrey[a)]
Department of Chemistry, National University of Ireland-Maynooth, Maynooth, County Kildare, Ireland

Narrow linewidth emission features observed in the near-UV following y ^{6}P state excitation of atomic manganese isolated in the solid rare gases are assigned to b ^{4}D and a ^{4}P states. These states arise from the $3d^54s^2$ electronic configuration, identical to that of the ^{6}S ground state, and the origin of the narrow linewidths. Two thermally stable sites, labeled blue and red on the basis of their position in absorption spectra, are occupied by atomic Mn in Ar and Kr while a single site is present in Xe. The red site produces a single, narrow line emission for the b ^{4}D state at 329 nm. In contrast, a lineshape analysis of the complex blue site b ^{4}D state emission between 331 and 332 nm reveals the occurrence of three zero phonon lines (ZPLs). Millisecond emission decay curves recorded for these features are found to be complex, requiring double and triple exponential fit functions. The origins of the complex decays and multiple ZPLs are shown to arise from weak crystal field splitting (CFS) of the J=7/2 spin-orbit level of the b ^{4}D state of atomic Mn isolated in the blue site of the solid rare gases. Fields of cubic symmetry are capable of inducing splitting for J>3/2 so atoms isolated in both single vacancy and tetravacancy sites in the fcc lattices of the solid rare gases are prone to this effect. b ^{4}D state emission is also produced following y ^{6}P excitation for Mn atoms occupying the red sites in Ar and Kr. However, Mn atoms isolated in the larger tetravacancy sites have small matrix shifts and do not exhibit any CFS. The magnitudes of the weak CF splittings are shown to depend on both the excited state electronic configurations $3d^54s^2$ b ^{4}D and $3d^64s^1$ a ^{4}D states and the size of the matrix site occupied by atomic Mn. © *2010 American Institute of Physics.* [doi:10.1063/1.3374030]

I. INTRODUCTION

Previous studies of the luminescence spectroscopy of metal atoms isolated in the solid rare gases have shown that emission linewidths depend very strongly on the electronic configurations involved in the transitions. Thus, $p \rightarrow s$ transitions are now well known[1] to be broad, exhibiting large Stokes'-shifted emission while $d \rightarrow s$ transitions are narrow and unshifted from their gas phase positions. This behavior emerged from the studies presented by Bondybey[2] on atomic Ca, Pellin *et al.*[3] on Cr and Mo, Nixon and co-workers[4] on Fe, Co, and Ni atoms, the groups of Kolb[5] and Ozin[6] on Cu, Ag, and Au, and by the Maynooth group on Zn,[7] Cd,[8] and Hg.[9] Recently, we reported the luminescence spectroscopy[10,11] of matrix-isolated atomic Mn and found that while these conclusions are generally correct, another factor playing a significant role in determining the emission linewidth is the site of isolation. Contrary to expectation, it was established that certain sites are capable of considerable broadening on $d \rightarrow s$ transitions while others exhibit the normal characteristics of narrow and unshifted emission from the gas phase position. In a recent molecular dynamics study of matrix-isolated atomic sodium[12] the nature of the sites occupied by this large atom was examined. As anticipated, large tetravacancy (TV) and hexavacancy sites were found in simulated depositions for Na in Ar and Kr. However, upon

prolonged laser excitation novel "violet" sites were generated in these solids which were attributed to the "cramped" occupancy of sodium atoms in single vacancy (SV) sites.

We now extend a study of the effects of the trapping site on matrix-isolated metal atoms, by analyzing the splitting observed on the narrow emissions of distinct spin-orbit levels in certain sites and the complete absence of splitting in other sites. This study, conducted on the near-UV emission spectroscopy of atomic Mn, reveals the existence of weak crystal field splitting in the smaller sites of the solid rare gases. The near-UV emission bands studied result from photoexcitation of the strongest resonance, *viz.*, the $[Ar]3d^54s4p$ y ^{6}P$\leftarrow[Ar]3d^54s^2$ a ^{6}S transition[13] at 279.827 nm in the gas phase.[13] The $3d^54s4p$ configuration gives rise to the y ^{6}P and the z ^{6}P states, both of which are accessible in fully allowed electric-dipole transitions from the ^{6}S ground state. In previous matrix absorption[14] and magnetic circular dichroism (MCD) (Ref. 15) studies by Vala and co-workers, strong atomic Mn absorption bands were observed close to the position of these two gas phase transitions. However, the spectra were complex indicating occupancy of Mn atoms in multiple sites. More recently, excitation spectra[16] recorded by our group indicated that atomic Mn isolated in solid Kr occupies only two distinct thermally stable sites. The blue site, tentatively attributed to SV occupancy, produces y ^{6}P state absorption at 279.2 nm and the red, TV site absorbs at 284 nm. The corresponding bands are centered at 273 and 278 nm in the Mn/Ar system. Atomic Mn exists in a
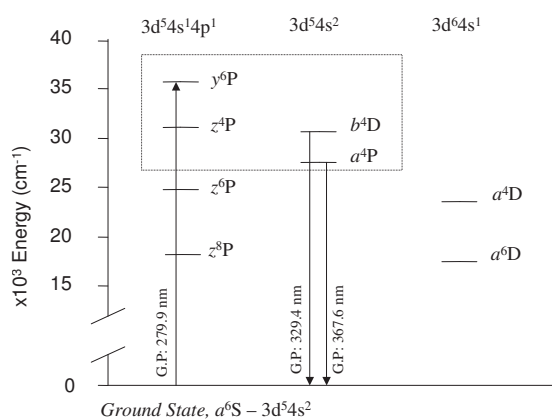
a)Electronic mail: john.mccaffrey@nuim.ie.

FIG. 1. A schematic of the energy levels of gas phase atomic manganese (Ref. 13). Luminescence in the present study is produced with photoexcitation of the fully allowed $y\,^6P_{5/2} \leftarrow a\,^6S_{5/2}$ transition, occurring at 35 726 cm^{-1} (279.91 nm) in the gas phase, is indicated by the upward arrow. The area of the diagram shown in the dotted box highlights the excited states that exist immediately below the $y\,^6P$ state and which are accessible in relaxation occurring after $y\,^6P \leftarrow a\,^6S$ excitation. The gas phase transitions from the $a\,^4P$ and $b\,^4D$ levels, which have the same $3d^54s^2$ configuration as the ground $a\,^6S_{5/2}$ state, are of particular importance to the present study. The wavelengths of these transitions are shown by the downward arrows.

single thermally stable site in xenon matrices, producing absorption at 288.2 nm. The red site greatly dominates in Ar, while the blue site only slightly dominates in Kr.

The excited states of atomic manganese energetically accessible with $y\,^6P$ state excitation are shown in Fig. 1. Eleven excited states occur to lower energy than the $y\,^6P$ of which the $z\,^4P$, $b\,^4D$, $a\,^4P$, $z\,^6P$, $a\,^4D$, $z\,^8P$, and $a\,^6D$ are shown. The luminescence produced with excitation of the lower energy $z\,^6P \leftarrow a\,^6S$ resonance transition involves only the last four states. Since this work has been presented in an earlier paper,[10] analysis of the emission from these lower energy states will not be repeated in this presentation, even though these bands are also produced with $y\,^6P \leftarrow a\,^6S$ excitation. Interested readers are referred to Ref. 10 for details of the low energy emission bands. As indicated in Fig. 1, excitation of the $y\,^6P$ state gives access to the $b\,^4D$ and $a\,^4P$ states which have the same $3d^54s^2$ electronic configuration as the ground $a\,^6S$ state. These states would be expected to produce narrower lines than the lower energy $3d^64s^1$ $a\,^4D$ and $a\,^6D$ states, both of which involve $d \rightarrow s$ orbital transitions. In the present contribution, the site dependence of the emission from the $b\,^4D$ and $a\,^4P$ states is analyzed in detail.

This paper is structured as follows. Firstly, steady-state emission spectra recorded with continuous lamp excitation of the absorption features assigned to the $y\,^6P \leftarrow a\,^6S$ transition of atomic Mn isolated in the rare gases Ar, Kr, and Xe are presented. Excitation spectra recorded monitoring the resulting emission features are then presented which allow site identification. With this information, high-resolution emission spectra allow characterization of the observed emission lineshapes for Mn atoms isolated in specific sites. Excited state lifetime measurements, made with pulsed laser excitation, are used to assign the recorded emission bands to transitions of atomic manganese. Lineshape analyses conducted with the optical W_p function[17] are used to locate the zero

phonon lines (ZPLs) in complex emission bands. A crystal field analysis of the emission bands is conducted for Mn atoms isolated in sites of cubic symmetry. A general analysis of the presence of CFS on the lower energy $a\,^4D$ and $a\,^6D$ states is presented for the Mn atom occupying both small and large matrix sites.

II. EXPERIMENTAL

The experimental setup used for recording excitation and emission spectra has been described elsewhere.[9,10,16] Briefly, a 0.5 m (Acton Research Corporation, model ARC SP500i) monochromator fitted with three gratings[10] and a photon counting (Hamamatsu R928-P) photomultiplier tube cooled to $-20\,^\circ$C were employed to record emission from Mn/RG samples. Steady-state excitation was from a deuterium lamp (Hamamatsu L6310 and a Cathodeon C713 power supply)[9] dispersed by a 0.3 m (ARC SP300i) monochromator.[9] Pulsed excitation was achieved by doubling the output of a (Quantel, model TDL-90) dye laser, pumped by the second harmonic of a 10 Hz (Quantel, model YG-980E) Nd:YAG (yttrium aluminum garnate) laser.[9] The wavelengths required for site-specific laser excitation of atomic manganese in the 273–288 nm spectral region were produced by doubling the output of the rhodamine 590 dye. A potassium dihydrogen phosphate crystal (Quantel, DCC3) was used for frequency doubling while a quartz crystal (Quantel, QCC1) was used to compensate for the walk of the resultant beams.[10] Wavelength separation of the UV beam from the dye laser beam was achieved with a Pellin–Broca prism. Time resolved emission spectra (TRES) were recorded using an intensified gated iCCD (intensified charged coupled device) detector (Andor Technologies, model iStar DH720) mounted on the SP500i imaging spectrograph.[10] Nanosecond decay curves were obtained by taking slices of the TRES at specific emission wavelengths. Emission decays on microsecond and longer timescales were recorded, as described elsewhere,[9] with photon counting using a 2 GHz (FastComTec, model 7886) multichannel scaler.

The gas handling system and vacuum apparatus used in the preparation of Mn/RG matrix samples has been described in previous publications from our group.[10,16] Manganese vapor was generated by electron bombardment of Mn metal contained in a Mo crucible. The emission spectra reported in this study were recorded in the most dilute Mn/RG samples formed. As shown in our previous absorption work,[16] these samples contain predominately isolated atomic manganese. Because of the extent of the site and state-specific emissions observed in the Mn/RG matrix systems, only spectra recorded in annealed samples are presented in this contribution.

III. RESULTS AND ANALYSIS

A. Emission

A summary of the near-UV emission features produced[18] with excitation of the $y\,^6P \leftarrow a\,^6S$ transition is presented in Fig. 2 for the Mn/Ar, Mn/Kr, and Mn/Xe systems. The recorded emission bands fall into two main categories; those around 330 nm and those near 370 nm. In Xe an additional
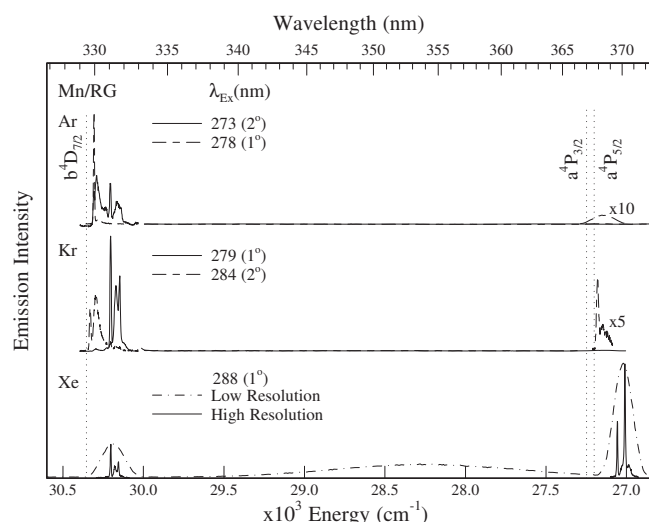
FIG. 2. Emission spectra recorded at 12 K for the Mn/Ar, Mn/Kr, and Mn/Xe systems with site-selective lamp excitation of the Mn $y\,^6P \leftarrow a\,^6S$ transition. The excitation wavelengths used are indicated on the left by λ_{Ex} in wavelength units. The relative amounts of the red and blue sites occupied in solid Ar and Kr are presented in brackets as either primary (1) or secondary (2). The effect of resolution is shown for the Mn/Xe data in lowest trace. All spectra were recorded following Mn/RG sample annealing. The spectral positions of the gas phase transitions of atomic Mn are shown by the dashed vertical lines.

FIG. 3. Luminescence spectra recorded at 12 K for the Mn/RG systems in the region of the gas phase $y\,^6P \leftrightarrow a\,^6S$ transition of atomic manganese at 279.9 nm (35 725.85 cm^{-1}), indicated by the dotted vertical line. The excitation wavelengths used to record the emission spectra are indicated in the middle by λ_{Ex} in nanometer units. Excitation spectra are presented for each system monitoring the emission bands at wavelengths indicated as λ_{Em} (nm). The Mn/Ar, Mn/Kr, and Mn/Xe samples were deposited at 12 K and annealed to 30, 37, and 62 K, respectively. The inset shows the decay profile recorded with iCCD detection of the broad Mn/Xe emission centered at 356 nm. The temporal profile of the pulsed dye laser is indicated by the triangles. The result of fitting the decay profile with a trial single exponential function convoluted with the laser temporal profile is also presented.

broad band, evident in the low resolution scan on the bottom of Fig. 2, is centered at 354 nm. It is obvious in Fig. 2, that the 330 nm bands are only slightly redshifted from the $b\,^4D_{(J=7/2)} \rightarrow a\,^6S_{5/2}$ transition occurring at 329.44 nm in the gas phase. The 370 nm bands are similarly redshifted from the $a\,^4P_{(J=5/2)} \rightarrow a\,^6S_{5/2}$ transition at 367.63 nm. Both sets of bands at 330 and 370 nm are spectrally narrow (<10 cm^{-1}) and, due to the small matrix shifts, can be assigned with confidence to the $b\,^4D$ and $a\,^4P$ states, respectively. The width of the Mn/Ar band centered at 368.5 nm arises because of the low resolution used to record this weak feature—its true lineshape has not been determined in this study. The effect of the resolution used is illustrated by the Mn/Xe spectra shown on the bottom of Fig. 2. In the following sections, luminescence of the $3d^5 4s 4p\ y\,^6P$ state and details of the emission features resulting from the $3d^5 4s^2\ b\,^4D$ and $3d^5 4s^2\ a\,^4P$ states are presented. Because the emission features in the three rare gases are observed to be site-specific, the results will be reported separately for the thermally stable red and blue sites.

B. Mn($y\,^6P$)/RG fluorescence

The most pronounced difference, evident in Fig. 2, between Mn/Xe and the other Mn/RG systems is the existence of the broad, featureless band centered at 354 nm. The state assignment of this band is not as straightforward as the narrow bands at 330 and 370 nm. To obtain an assignment for the 354 nm band, its excitation spectrum and emission decay were recorded, the results of which are shown in Fig. 3. The fully allowed $y\,^6P \leftrightarrow\,^6S$ resonance transition occurs at 279.9 nm in the gas phase and the Mn/Xe excitation band at 288.2 nm, shown on the bottom left in Fig. 3, corresponds to the previously recorded atomic absorption. An emission de-
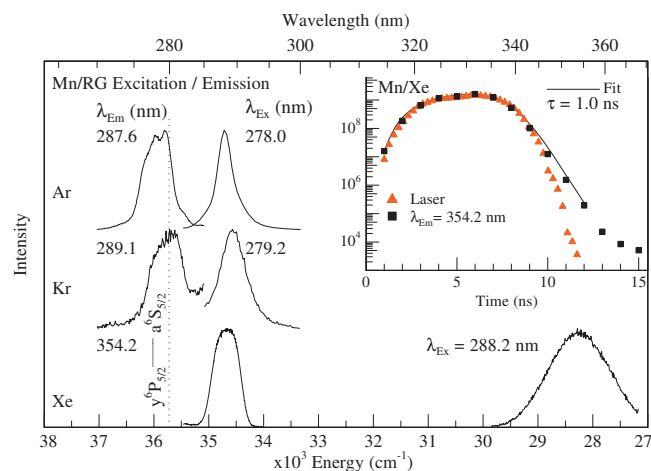
cay profile extracted at 356 nm from the TRES indicates a lifetime of 1.0 ns for this band as shown in the inset of Fig. 3. The gas phase lifetime[19] of the $y\,^6P$ state of atomic manganese is 2.6 ns, and the recorded matrix value closely matches this value when it is corrected for the effective field of the solid. Accordingly, we assign the broad 354 nm emission band in Mn/Xe to $y\,^6P \rightarrow a\,^6S$ fluorescence.

The corresponding $y\,^6P$ state emission bands of Mn/Ar and Mn/Kr are at 287.6 and 289.1 nm, respectively, as shown in Fig. 3. The emission bands in these two systems are very weak relative to the narrow bands presented in Fig. 2. A comparison of the Mn/Ar and Mn/Kr fluorescence excitation spectra with the absorption spectra shown in Fig. 5 of Ref. 16 reveals that only the dominant absorption sites have been picked up in the $y\,^6P$ state excitation scans. It is also evident in Fig. 3 that the emissions in Mn/Ar and Mn/Kr exhibit much smaller Stokes shifts than the Mn/Xe system. Values of approximately 1250 cm^{-1} have been determined in Ar and Kr while it is 6450 cm^{-1} in Xe. However, the nanosecond decay times extracted for the bands in the Ar and Kr systems indicate they also arise from the $y\,^6P \rightarrow a\,^6S$ transition.

C. 330 nm luminescence

1. State assignments

The intense, structured emission bands in the 330 nm spectral region are shown in Fig. 4 on an expanded scale revealing striking resemblances in the three hosts studied. The labels "blue site" and "red site" used for the emission in this figure pertain to relative spectral positions of their excitation/absorption bands (reported previously)[10] and not their emission locations. Assignment of the sharp, red site bands at 329.96 and 329.70 nm in Ar and Kr, respectively, to
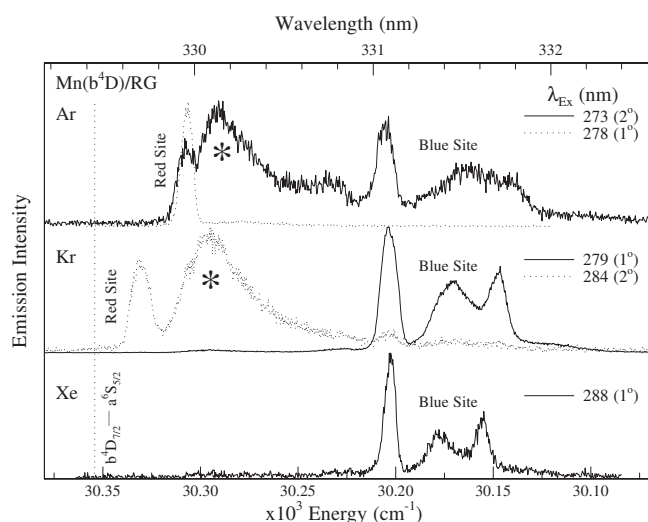
FIG. 4. Site dependence of the high-resolution emission spectra recorded at 12 K in the vicinity of the gas phase $b\ ^4D \leftrightarrow a\ ^6S$ transition following site-specific (red/blue) $y\ ^6P \leftarrow a\ ^6S$ excitation of atomic Mn isolated in Ar, Kr, and Xe. The spectral position of the lowest energy $J=7/2$ spin-orbit level of the $b\ ^4D$ state is indicated by the dotted vertical line at 329.44 nm (30 354.21 cm^{-1}). Emission produced with blue [single substitutional (SV)] site and red (TV) site excitation in Ar, Kr, and Xe are presented as solid and dotted lines, respectively. The excitation wavelengths used are indicated by λ_{Ex} in wavelength units. The asterisks identify emission bands produced with excitation of a thermally unstable matrix site.

$b\ ^4D_{(J=7/2)} \rightarrow a\ ^6S_{5/2}$ emission of atomic manganese is direct as this transition, shown by the dotted vertical line, occurs at 329.44 nm in the gas phase. The origin of the three resolved features present between 331 and 332 nm cannot, however, be immediately established. For instance, other spin-orbit ($J=1/2$, 5/2, and 3/2) levels of the $b\ ^4D$ state exist but they are at higher energy and with intervals in the gas phase (8 and 6 cm^{-1}) quite different to the observed matrix splittings of 26 and 21 cm^{-1}. Previous data obtained by our Group[20] with direct excitation of the forbidden $a\ ^6D_J \leftarrow a\ ^6S$ transition demonstrate that the gas phase splitting between spin-orbit levels is maintained in the matrix environment. Inspection of Fig. 1 reveals that no other D states of atomic Mn occur in the near-UV region. The $z\ ^4P_{(5/2)} \leftrightarrow a\ ^6S_{5/2}$ transition occurs at 322.57 nm (31 001 cm^{-1}) in the gas phase[13] but since this excited state arises from the "triplet-like" $3d^54s4p$ electronic configuration, this open p-shell configuration should produce a broad, strongly Stokes-shifted emission in solid Xe, not the narrow lines observed. The corresponding low energy "tripletlike" $3d^54s4p\ z\ ^8P$ state was not observed in solid Xe following direct laser excitation.[16] By a process of elimination the 331–332 nm matrix emission features observed in all three solid hosts must arise from the $J=7/2$ level of the excited $b\ ^4D$ state of atomic Mn but the origin of the complex structure on the blue site emission requires analysis which will be presented next.

2. Blue site emission

Mn/Xe offers the ideal starting point to analyze the bands in the 331–332 nm range since all the emission features in this system arise from a single site. The blue site

emission in Mn/Xe, shown by the solid-trace on the bottom of Fig. 4, exhibits three narrow features at 331.09, 331.38, and 331.6 nm. The most intense feature at 331.09 nm (30 203 cm^{-1}) exhibits a full width at half maximum (FWHM) of 6.4 cm^{-1} and a red matrix shift of 151 cm^{-1} from the $b\ ^4D_{(J=7/2)} \rightarrow a\ ^6S_{5/2}$ gas phase position. The emission decay curves recorded for the structured features were all in the 1 ms region. Adequate fitting required double exponential functions, the details of which are given in Table I and shown in the bottom panel of Fig. 5. Temperature dependent emission spectra for these features are presented in Fig. 5. Inspection of the Mn/Xe data presented in the lower panel reveals that at 24 K, the highest and lowest energy features lose some intensity with respect to the central component. At the higher temperature, an additional narrow feature (FWHM 10 cm^{-1}) is evident at 330.8 nm (30223 cm^{-1}), blueshifted by about 20 cm^{-1} from the most intense feature in the 12 K spectrum. On returning to 12 K the original spectrum was regained indicating the temperature dependence observed was completely reversible. This behavior is characteristic of resolved phonon structure.

The blue site 331 nm emission features in Kr and Xe matrices reveal very similar splitting patterns when recorded under high resolution. Thus, as shown in Fig. 4, both Mn/Xe and Mn/Kr exhibit a dominant sharp (FWHM=9.5 cm^{-1}) line at 331.087 nm (30 203.5 cm^{-1}) and a pair of resolved lines at lower energy with approximately half the intensity of the blue feature. The two red bands are centered at 30 173 and 30 147 cm^{-1} in Kr and at 30 179 and 30 157 cm^{-1} in Xe. With the exception of the emergence of hot emission bands, doubling the temperature had no effect on the line positions and produced only a slight increase in the relative intensity of the central band. The narrow linewidths and the lack of pronounced temperature dependence of the three resolved bands indicate a system with very weak electron-phonon coupling. Accordingly, the three bands of the blue site present in Fig. 5 are identified as three ZPLs, with weak phonon sidebands responsible for the unresolved background.

To determine the actual positions of the three ZPLs in the Mn/Kr and Mn/Xe systems, lineshape analyses were conducted on the recorded emission bands with the W_p optical function. This function, described in detail by Struck and Fonger,[17] provides an analytic expression for the Franck–Condon intensity factors for displaced harmonic oscillators. It assumes the dominance of a single phonon mode with a frequency $\hbar\omega$, an average value for the ground and excited electronic states coupled in the transition. The W_p lineshape analysis allows, as shown in our earlier work,[9] identification of the band origin, $\nu_{0,0}$, i.e., the ZPL and an assessment of the electron-phonon coupling strength S, for the electronic transition involved. The starting point for the W_p lineshape fit is the selection of a value for the phonon frequency ($\hbar\omega$) required to transform the recorded spectrum into phonon units, p.

The presence of resolved hot emission bands in the high temperature spectra allows direct measurement of the magnitude of the phonon frequency $\hbar\omega$. Values of 25 and 19 cm^{-1} were identified in this manner for Mn/Kr and Mn/

TABLE I. Photophysical characteristics and excited state assignments of the emission features produced with excitation of the $3d^5 4s 4p$ y ^{6}P $\leftarrow 3d^5 4s^2$ a ^{6}S transition of atomic manganese isolated in the two thermally stable sites in Ar and Kr and the single site in Xe. λ indicates the emission band center in units of nanometers. The full width at half-maximum intensity of the emission features is denoted by Δ and the matrix shift by δ. Both quantities are provided in wavenumber (cm^{-1}) units. The observed excited state radiative lifetimes are presented where τ_{obs} indicates the lifetime of the dominant decay component at 12 K. The question marks indicate state assignments that are only tentative.

State	ν (cm^{-1})	Band λ (nm)	Δ (cm^{-1})	δ (cm^{-1})	τ_{obs}
		Mn gas phase			
y ^{6}P$_{3/2}$	35 690	280.19	$\cdots$	$\cdots$	2.6 ns
b ^{4}P$_{5/2}$	33 825	295.64	$\cdots$	$\cdots$	
z ^{4}P$_{5/2}$	31 001	322.57	$\cdots$	$\cdots$	
b ^{4}D$_{7/2}$	30 354	329.45	$\cdots$	$\cdots$	
a ^{4}P$_{5/2}$	27 202	367.62	$\cdots$	$\cdots$	
		Mn/Ar blue (2°) site			
b ^{4}D$_{7/2}$	30 206	331.06	10	-148	$\cdots$
a ^{4}P (?)	27 137	368.5	$\cdots$	-65 (?)	$\cdots$
		Mn/Kr blue (1°) site			
y ^{6}P	34 551	289.42	468	-1139	<1 ns
b ^{4}D$_{7/2}$	30 204	331.08	9.4	-150	2.78 ms
		Mn/Xe			
y ^{6}P	28 234	354.2	1392	-7456	1 ns
b ^{4}D$_{7/2}$	30 203	331.09	6.4	-151	1.51 ms
a ^{4}P$_{3/2}$	27 057	369.59	6.4	-191	12.6 ms
a ^{4}P$_{5/2}$	27 010	370.23	6.7	-192	15.4 ms
		Mn/Ar red (1°) site			
y ^{6}P	34 718	288.03	322	-972	<1 ns
b ^{4}D$_{7/2}$	30 307	329.96	6.8	-47	794 μs
		Mn/Kr red (2°) site			
b ^{4}D$_{7/2}$	30 331	329.70	10	-23	1.33 ms
a ^{4}P	27 181	367.9	10	-21	1.36 ms

Xe, respectively. A satisfactory fit was obtained in the Mn/Kr system with S=0.23 and three ZPLs at 30 204, 30 171, and 30 149 cm^{-1}. The results of this fit are shown on the left in Fig. 6 at 12 K and on the right for 22 K. The high temperature fit correctly describes the intensity increase of the "hot" emission at 30 229 cm^{-1} to the blue of the ZPL and otherwise, little change in the emission profile. The lack of a strong temperature dependence is a direct result of the very small S value extracted in the fit. In Mn/Xe a satisfactory fit was obtained with $\hbar\omega$=19.0 cm^{-1}, S=0.26, and three ZPLs at 30 204, 30 177, and 30 157 cm^{-1}. For Mn/Ar the W_p lineshape analysis was not as reliable due to the weakness of the blue site emission, however, an acceptable fit was obtained with $\hbar\omega$=32 cm^{-1}, S=0.20, and ZPLs at 30 205, 30 165, and 30 144 cm^{-1}. For a given matrix system all the fits were conducted with the same S and $\hbar\omega$ values for the three ZPLs identified. The relative intensity of the ZPLs was an adjustable parameter but was found to be 2:1:1 for the 7/2 level of the excited b ^{4}D state. The parameters extracted from the W_p fits of the blue site emission in the three rare gases studied are collected in Table II.

3. Red site emission

With red (TV) site excitation in solid Ar and Kr single, intense peaks are observed at 329.96 and 329.7 nm, respectively, as shown by the dotted traces in Fig. 4. Energetically
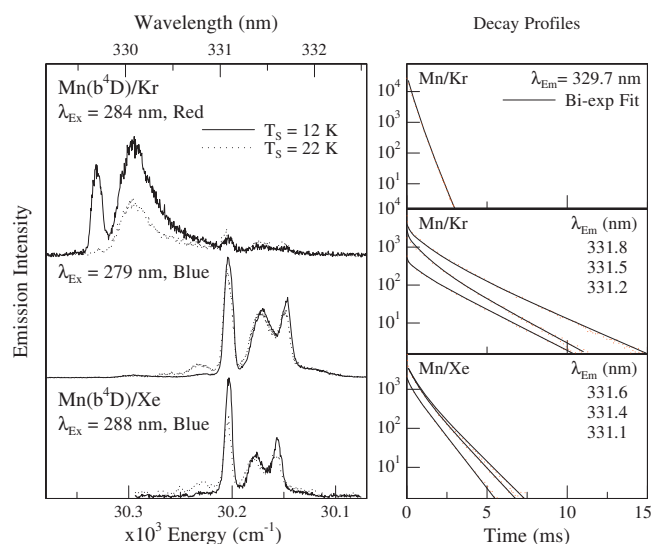

FIG. 5. The temperature dependence of high-resolution emission spectra recorded in the vicinity of the gas phase b ^{4}D$_{7/2} \leftrightarrow a$ ^{6}S transition of Mn isolated in solid Kr and Xe following site-specific (red/blue) y ^{6}P $\leftarrow a$ ^{6}S pulsed laser excitation. The blue site emissions in Kr and Xe exhibit little temperature dependence while the narrow red site 329.7 nm emission in Kr is nearly completely removed at 22 K. T_s denotes the temperature at which the spectra were recorded and λ_{Ex} indicates the excitation wavelength. On the right emission decay profiles of the dominant thermally stable bands recorded at 12 K using photon counting and multichannel scaling are shown as dots. The results of trial biexponential fits of the decay profiles are presented as solid lines.
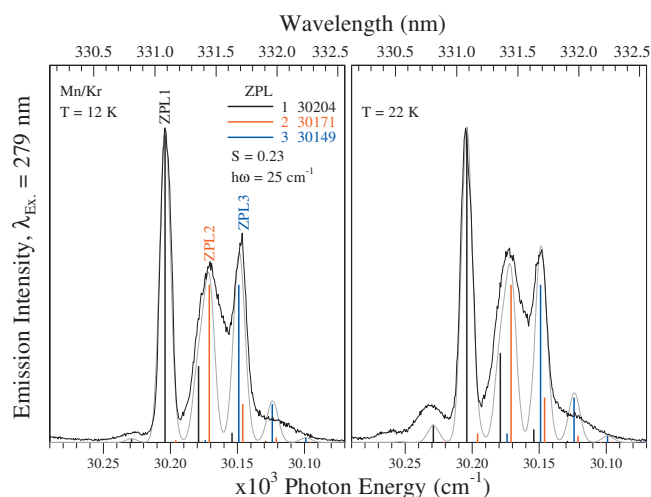
FIG. 6. Simulations of high-resolution $b\,^4D_{7/2}$ state emission spectra recorded at 12 and 24 K with pulsed laser excitation at 279 nm of the thermally stable, blue site occupied by atomic Mn in solid krypton. Fits of the resolved phonon features were generated with the W_p line shape functions using three ZPLs whose values are indicated in the plot as ZPL1, ZPL2, and ZPL3 in wavenumber units. The relative intensities of the three ZPLs were 2:1:1, as indicted by the height of the three strongest vertical lines shown in black, red, and blue. Simulations of the emission band profiles were generated by convoluting the line distributions in each of the three W_p fit functions, described in the text, with 6.6 cm^{-1} (FWHM) Gaussians. The presence of hot-phonon emission is most evident on the high energy side of ZPL1 in the 22 K scan shown on the right.

the closest transition of atomic manganese is the $b\,^4D_{(J=7/2)}$ $\rightarrow a\,^6S_{5/2}$ transition, which occurs at 329.44 nm in the gas phase. Thus, the 329.96 nm emission in Ar clearly originates from the J=7/2 level of the excited $b\,^4D$ state of atomic Mn. Decay profiles recorded monitoring the narrow emission in Ar and Kr were fit with double exponential functions. The dominant decay components extracted for Ar and Kr were of

the order of 1 ms reinforcing the assignment to the spin and parity forbidden $b\,^4D_{(J=7/2)} \rightarrow a\,^6S_{5/2}$ transition of atomic Mn. Table I presents the photophysical properties of the 330 nm emission features following red site excitation in solid Ar and Kr. Emission spectra recorded for Mn/Kr at 22 K, shown in the top left panel of Fig. 5, indicate that the narrow emission at 329.7 nm is completely removed at high temperature. It is noteworthy that the $b\,^4D$, J=7/2 state emission shows no discernable structure for Mn atoms in the larger red site present in Ar and Kr. The linewidth of the bands present in the spectra is limited by the 5 cm^{-1} resolving power of the 0.5 m monochromator used to record emission.

D. 370 nm luminescence

1. Blue site emission

Excitation of $y\,^6P$ state Mn in solid Xe also produces the two narrow emission features at 369.59 and 370.23 nm shown in Fig. 7. The closest gas phase transitions to the pair of sharp emission features at 370 nm are the $a\,^4P_{3/2,5/2}$ $\rightarrow a\,^6S$ transitions occurring at 367.00 nm (27 248.00 cm^{-1}) and 367.62 nm (27 201.54 cm^{-1}), respectively. The difference in energy between the two matrix peaks is 46 cm^{-1} identical, within the accuracy of our emission monochromator, to the gas phase splitting between the $a\,^4P_{3/2}$ and $a\,^4P_{5/2}$ atomic transitions (46.46 cm^{-1}). Thus, these two intense peaks at 369.59 and 370.23 nm are assigned as emission from the J=3/2 and J=5/2 spin-orbit levels, respectively, of the $a\,^4P$ state-both transitions in Xe exhibit a redshift of 191.5 cm^{-1} as illustrated in Fig. 7. The $a\,^4P$ state has the same $3d^54s^2$ electronic configuration as the ground state, this accounts for the narrow lineshapes observed. The emission decay curves of both features were satisfactorily

TABLE II. Spectral positions for the narrow-band emission features assigned to the $b\,^4D_{7/2} \rightarrow a\,^6S$ and $a\,^4D_{7/2} \rightarrow a\,^6S$ transitions of atomic manganese produced with excitation of the $y\,^6P$ and $z\,^6P$ transitions, respectively. The $b\,^4D_{7/2}$ emission is carried by Mn atoms isolated in substitutional (blue) sites in Ar, Kr, and Xe, whereas the $a\,^4D_{7/2}$ presented in a previous publication (Ref. 10) results from excitation of Mn atoms isolated in tetravacancy (red) matrix sites. ν indicates the emission band center in wavenumber units. The results of W_p fits of the emission band profiles allowed the assignment of ZPL. Crystal field splitting patterns is denoted by CFS and the matrix shift by δ-both in wavenumber (cm^{-1}) units.

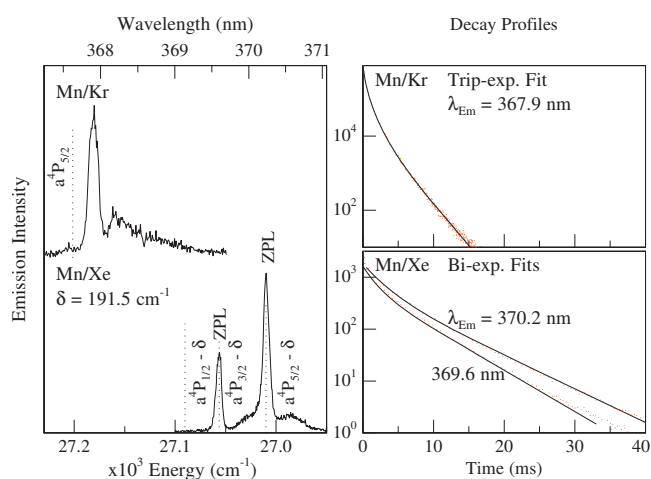| System	Electronic config.	ν (cm^{-1})	Assignment	CFS (cm^{-1})	δ (cm^{-1})
		Mn($b\,^4D_{7/2}$)/RG-blue site			
Mn/Ar	$3d^54s^2$	30 205	ZPL 1		−148
		30 168	ZPL 2	37	
		30 141	ZPL 3	27	
Mn/Kr	$3d^54s^2$	30 204	ZPL 1		−150
		30 171	ZPL 2	33	
		30 149	ZPL 3	22	
Mn/Xe	$3d^54s^2$	30 204	ZPL 1		−151
		30 177	ZPL 2	27	
		30 157	ZPL 3	20	
		Mn($a\,^4D_{7/2}$)/RG-red site			
Mn/Ar	$3d^64s^1$	23 388	ZPL 1		+91
		23 358	ZPL 2	30	
		23 352	ZPL 3	6	
Mn/Kr	$3d^64s^1$	23 374	ZPL 1		+77
		23 342	ZPL 2	32	
		23 328	ZPL 3	14	

FIG. 7. Spectral and temporal characteristics of the sharp emission present in Kr and Xe near 370 nm in the vicinity of the gas phase $a\ ^4P_J \leftrightarrow a\ ^6S$ transitions of Mn. The vertical dotted line on the upper left indicates the gas phase position of the $a\ ^4P_{5/2} \leftrightarrow a\ ^6S_{5/2}$ transition indicating a very small shift for the red site emission in Kr. The dotted lines presented in the lower right show the three spin-orbit levels of the $a\ ^4P_J$ state redshifted by $\delta = 191.5$ cm^{-1}, allowing easy identification of the pair of lines on the Mn/Xe system as the $a\ ^4P_{3/2}$ and $a\ ^4P_{5/2} \leftrightarrow a\ ^6S_{5/2}$ transitions, respectively. On the right decays of the three dominant emission bands are shown. The results of trial multiexponential fits of the decay profiles are presented as solid lines.

fitted with double exponential functions as shown on the bottom right of Fig. 7. The major component shows decay times of 12.5 and 15.4 ms as listed in Table I.

2. Red site emission

An emission feature is observed at 368.2 nm in Mn/Kr following red site excitation at 284 nm (see Fig. 2). The $a\ ^4P_{(J=5/2)} \rightarrow a\ ^6S$ transition of atomic manganese occurs at 367.62 nm in the gas phase, thus the 368.2 nm emission feature present in Kr is assigned as emission from the $a\ ^4P_{(J=5/2)}$ excited state showing a matrix shift of 63 cm^{-1} from the gas phase. Fitting the decay profile of this feature required a triple exponential function the result of which is presented in Fig. 7 and the decay times are provided in Table I. No emission feature is observed in this region following blue site excitation in Kr.

In Mn/Ar a weak emission band is observed at 368.4 nm following red site excitation (see Fig. 2) and due to its proximity to the gas phase $a\ ^4P_{(J=5/2)} \rightarrow a\ ^6S_{5/2}$ transition must originate from the excited $a\ ^4P$ state of atomic Mn. Due to the low intensity of this feature, it was not possible to record a high-resolution spectrum to establish whether this feature is structured or not. No emission features were observed in this region following blue site excitation in Ar.

IV. DISCUSSION

A. Site occupancy

In a previous analysis[16] of the $y\ ^6P$, $z\ ^6P$, and $z\ ^8P$ absorption/excitation spectra of matrix-isolated atomic manganese, a connection was made between the blue sites in Ar and Kr and the single thermally stable site in Xe. This behavior was identified in the linear correlation of the gas phase—matrix shifts and the polarizabilities of the three rare

TABLE III. Predictions of the bond lengths and binding energies of the ground state Mn·RG (RG=Ar, Kr, and Xe) diatomics obtained with the LP method. For comparison the results of this method are also presented for the Mg·RG (Ref. 22) and Na·RG (Ref. 23) diatomics where high quality experimental data exist.

LP	R_e (Å)	D_e (cm^{-1})	Exp	R_e (Å)	D_e (cm^{-1})
			Mn		
Ar	4.48	84.8	⋯	⋯	
Kr	4.54	114.6	⋯	⋯	
Xe	4.63	156.6	⋯	⋯	
			Mg		
Ar	4.55	89.4		4.49	65
Kr	4.59	121.6		⋯	⋯
Xe	4.68	167.7		4.56	94
			Na		
Ar	5.07	79.8		5.01	41.6
Kr	5.08	115		4.92	68.4
Xe	5.12	171		4.95	117

gases. A similar correlation was found between the red sites in Ar and Kr. Currently, neither spectroscopic nor high level *ab initio* potentials exist for the ground states of the Mn·RG (RG=Ar, Kr, and Xe) diatomics, so the sites occupied by atomic manganese in rare gas matrices cannot be definitively identified. Despite this shortcoming, reliable bond lengths can be predicted for the Mn·RG diatomics from a knowledge of the dispersive forces in these molecules. A refinement of this approach has been presented by Luiti and Pirani[21] (LP). Using the ionization potentials and polarizabilities (α) of atomic Mn and the rare gas atoms, ground state bond lengths of 4.48, 4.54, and 4.63 Å are obtained for the Mn·RG diatomics. These values and LP predictions for bond lengths of the known Mg·RG (Ref. 22) and Na·RG (Ref. 23) diatomics are presented in Table III. It is evident in the comparisons shown there with experimental data that the LP method overestimates the bond lengths by only about 5%. The bond length predictions indicate strong similarities between the Mn·RG and Mg·RG systems and dissimilarities with the Na·RG system. Thus occupancy of metal atoms in smaller sites will be favored in the Mn/RG systems compared to what has been found in MD calculations[12] of the site occupancy in the Na/RG systems.

Consistent with these findings, the 288.2 nm band in Xe was attributed previously[16] by us to Mn atom occupying single substitutional sites (SV) and from the linear polarizability dependence of the blue site absorptions in Ar and Kr, these sites are similarly assigned. Based on Na/RG molecular dynamics calculations,[12] the red absorption bands in Ar and Kr are attributed to larger TV sites. In summary, the blue site $y\ ^6P$ state absorption/excitation bands in Ar, Kr, and Xe are attributed to SV site occupancy, while the red sites in Ar and Kr are ascribed to TV sites.

B. State assignments

Table I presents the photophysical characteristics and excited state assignments of the emission features produced with excitation of the $3d^5 4s 4p\ y\ ^6P \leftarrow 3d^5 4s^2\ a\ ^6S$ transition of atomic manganese. From the entries in this table it is

Correlation Diagram of octahedral Crystal Field
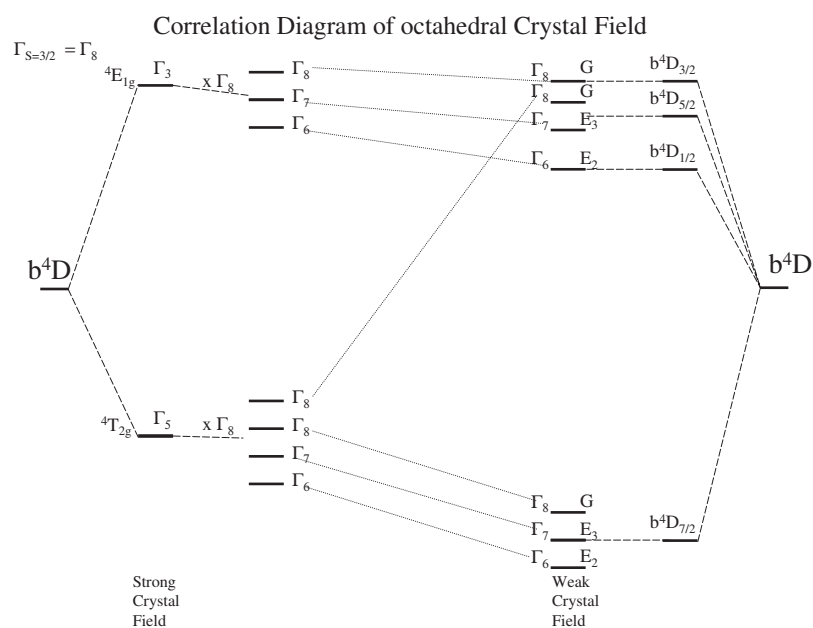
$\Gamma_{S=3/2} = \Gamma_8$

FIG. 8. A correlation diagram of the crystal field-induced fine structure of the J=7/2 spin-orbit level of the a ^{4}D$_{7/2}$ state in a cubooctahedral site. The weak field energy splittings depicted on the right are the gas phase for the spin-orbit levels shown to scale. The strong field splitting shown on the middle left is not to scale as the Mn-RG interaction energies are not known. The key result of this correlation diagram is the existence of three CF split levels (G, E_1, and E_2) with degeneracies of 4:2:2 for the J=7/2 spin-orbit level.

evident that the observed emissions fall into one of two distinct categories. Thus the broad emission bands at 288, 289, and 354 nm in Ar, Kr, and Xe respectively, all of which involve nanosecond lifetimes, are clearly resonance y ^{6}P $\rightarrow a$ ^{6}S transitions. Despite having similar lifetimes, the y ^{6}P state emission bands in Ar and Kr are quite different to Xe as the former exhibit moderate Stokes (~ 1000 cm^{-1}) shifts and linewidths (<500 cm^{-1}) but for Mn y ^{6}P state in Xe, much larger values ($\delta = 7500$, $\Delta = \sim 1400$ cm^{-1}) are observed. This contrasting behavior has already been observed in $p \rightarrow s$ transitions of several metal atom systems. The best documented[9] cases are the Hg, Cd, and Zn systems.

The second emission category has millisecond lifetimes and exhibits small matrix shifts from the gas phase transitions. Because of the small shifts and long lifetimes, quartet spin state assignments can be made even though gas phase lifetimes are not available. As indicated in Table I, the narrow bands in the 330 and 370 nm regions are assigned to the b ^{4}D and a ^{4}P states, respectively. Both of these states arise from the $3d^5 4s^2$ configuration identical to that of the ground a ^{6}S$_{5/2}$ state and entirely consistent with the observation of narrow emission lines. However, the extent of phonon structure on the b ^{4}D varies considerably between the sites occupied. In an attempt to identify the origin of this variation, the different lineshapes presented by these and other D states will now be assessed.

C. D state emission

Inspection of the spectra presented in Fig. 4 reveals that blue (SV) site excitation produces three very similar emission features in Ar, Kr, and Xe matrices. The most intense feature has a matrix shift of 150 cm^{-1} from the gas phase $3d^5 4s^2$ b ^{4}D$_{(J=7/2)} \rightarrow 3d^5 4s^2$ a ^{6}S$_{5/2}$ transition that is quite independent of the host. The W_p function fit of this emission, shown in Fig. 6 for Mn/Kr, was used successfully in the two other hosts. Overall, very weak electron-phonon coupling

(S=0.23) was used but most significantly, the existence of three resolved ZPLs was identified for the blue site, near-UV emission of all three hosts.

The presence of multiple ZPLs on a single spin-orbit level of the b ^{4}D state requires an investigation of the influence of the crystal field of the lattice site on the J=7/2 level. A correlation diagram, showing the origins of the crystal field splitting (CFS) in octahedral symmetry, is shown in Fig. 8 for all four spin-orbit levels of the ^{4}D state. The portion of the diagram appropriate for the b ^{4}D$_{7/2}$ state of matrix-isolated atomic manganese is on the bottom right hand side where the CFS is less than the spin-orbit splitting (SOS). Group theory predicts[24] that fields of cubic symmetry will produce three energetically distinct levels G, E_3, and E_2 with degeneracies[25] of 4, 2, and 2, respectively, from an original value of 8 (2J+1) for the J=7/2 level. If the CFS levels are populated statistically with y ^{6}P state excitation, then emission intensity ratios of 2:1:1 will occur. W_p fits of the recorded near-UV emission bands, shown in Fig. 6 for Mn/Kr, exhibit this intensity ratio for the three resolved ZPLs. Similar patterns were found for the blue site emissions in Xe and Ar with, as shown in Fig. 4, the magnitude of the splitting increasing in this series. In contrast, red site emission of the J=7/2 level in the b ^{4}D state exhibits a single, sharp ZPLs in both Ar and Kr only slightly shifted from the gas phase transition. If the red site emission bands have CFS, it is less than the 5 cm^{-1} resolution limit of our emission monochromator.

The intensity distribution of the ZPLs in the near-UV ($3d^5 4s^2$ b ^{4}D$_{J=7/2}$) blue site emission is reminiscent of the 428 nm bands previously observed by our group[10] for atomic Mn isolated in the red (TV) site of solid Ar and Kr. This emission, shown in Fig. 9 for Mn/Ar, is produced most efficiently with excitation of the z ^{6}P $\leftarrow a$ ^{6}S transition and has been assigned to the $3d^6 4s^1$ a ^{4}D$_{(J=7/2)}$ state. As the 428 nm bands also involves emission from the J=7/2 level, the same group theoretical analysis is valid here but tetrahedral symmetry is used for the TV (red) site occupied. The W_p fits of the emission at 12 and 25 K reveal, as shown in Fig. 9, small
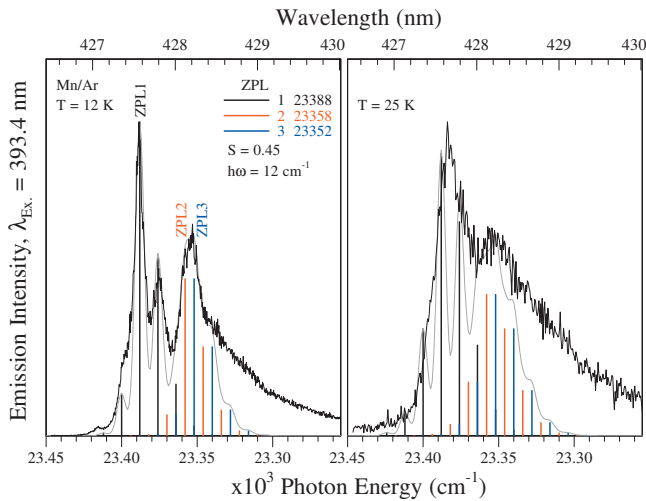
FIG. 9. A comparison of the high-resolution 428 nm a $^4D_{7/2}$ state emission recorded at two temperatures for the dominant red site of Mn/Ar with fits obtained with three W_p lineshape functions. The locations of the three ZPLs extracted are indicated on the plot in wavenumber units. The long, red wing unaccounted for in the simulation arises from broad, blue site emission centered at 440 nm.

S values of 0.45. As found for the near-UV blue site emission, the three ZPLs in the 428 nm emission exhibit the intensity ratios 2:1:1. In contrast, the blue site 440 nm emission of the $3d^64s^1$ a $^4D_{(J=7/2)}$ state is broad and featureless. This emission was previously fit[10] using a single W_p function with an S value of 6 indicating moderately strong electron-phonon coupling.
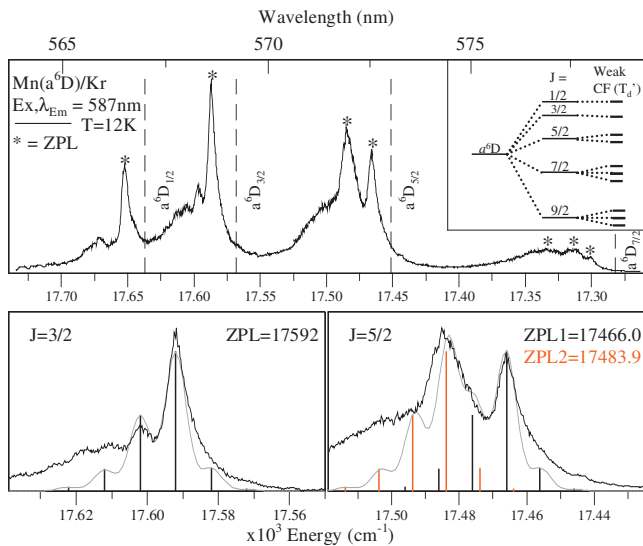

FIG. 10. High-resolution laser excitation spectra recorded at 12 K for the metastable a $^6D_{9/2}$ state emission of atomic manganese in an annealed Kr sample. The spectrum was recorded with rhodamine 590 monitoring the emission at 585.7 nm previously assigned to the a $^6D_{9/2} \rightarrow a$ $^6S_{5/2}$ transition. The dashed vertical lines indicate the gas phase positions of the excited spin-orbit levels of the a $^6D_J \leftrightarrow a$ ^6S state for J=1/2, 3/2, 5/2, and 7/2 levels. The presence of multiple zero-phonon lines in excitation is indicated by the asterisks. The inset on the top right illustrates the effect of a weak CF on the spin-orbit levels of the a ^6D_J states of atomic manganese isolated in a matrix site of tetrahedral symmetry (T'_d). The bottom panels present simulations of the resolved features in the Mn/Kr excitation band profiles recorded for the a $^6D_J \leftarrow a$ ^6S J=3/2 and 5/2 (left and right) recorded at 12 K. The locations of the ZPLs are shown by $\nu_{0,0}$ in wavenumber units. The band profiles were reproduced by centering Gaussian line shapes (FWHM 6.6 cm^{-1}) for the W_p distributions described in the text.

TABLE IV. Results of lineshape simulations of the Mn(a $^6D_J \leftarrow a$ ^6S)/Kr excitation and Mn(a $^4D_{7/2} \rightarrow a$ ^6S)/Kr and Ar emission spectra using the W_p optical function as described in the text. The W_p fit parameters $\nu_{0,0}$ and $\hbar\omega$ are presented in wavenumber cm^{-1} units while the Huang–Rhys factor S, is unitless. CFS of matrix-isolated atomic manganese is identified as the difference between adjacent zero-phonon lines for a given spin-orbit state.

J	S	ZPL (cm^{-1})	CFS	$\hbar\omega$ (cm^{-1})
		Mn(a ^6D_J)/Kr		
1/2	0.4	17 662	⋯	10
3/2	0.4	17 592	⋯	10
5/2	0.4	17 484	18	10
		17 466		
7/2	0.4	17 295	12	10
		17 307	21	
		17 328		
9/2	0.4	17 072.5	14.6	10
		17 087.1	18.5	
		17 105.6		
		Mn(a $^4D_{7/2}$)/RG		
Kr	0.4	23 328	14	10
		23 342	32	
		23 374		
Ar	0.45	23 352	6	12
		23 358	30	
		23 388		

In an earlier publication[20] we presented laser excitation spectroscopy of the metastable $3d^64s^1$ a ^6D state of Mn atoms recorded by monitoring emission at 585.8 nm. This emission wavelength corresponds to red site occupancy. With direct excitation of the a $^6D_J \leftarrow a$ ^6S transition the five spin-orbit levels of the a ^6D state were clearly identified because the gas phase splitting between spin-orbit levels was maintained in the matrix environment. In a recent W_p lineshape analysis conducted[26] on the distinct spin-orbit levels, multiple ZPLs were identified for J=5/2, 7/2, and 9/2 while single ZPLs were sufficient for the J=3/2 and 1/2 levels. A summary of the fits conducted is presented in Fig. 10 and the parameters extracted are collected in Table IV. This behavior is entirely consistent with group theoretical predictions of CFS for the five resolved spin-orbit levels in the range J =1/2 to 9/2. Small S values (=0.4) were extracted in these fits, indicative of weak electron-phonon coupling for the $3d^64s^1$ a ^6D state of atomic Mn in the red, TV site. The blue site emission of the $3d^64s^1$ a ^6D state is broad and located at 628 nm. A W_p fit of this emission band revealed an S value of 6 indicating moderately strong electron-phonon coupling in the smaller site.

V. CONCLUSIONS

Considering the above observations, a pattern emerges that the $3d^64s^1$ orbital occupancy produces narrow emission bands (a $^6D_{9/2}$/585.8 nm, a $^4D_{7/2}$/428 nm) with resolved CFS when the Mn atom is isolated in the larger (red) TV site. Conversely, broad, shifted emission (a ^6D/628 nm, a ^4D/440 nm) arises when Mn is in the smaller (blue) substitutional site. In contrast, the $3d^54s^2$ orbital occupancy produces resolved CFS emission when Mn is in the blue site

TABLE V. A summary of the combined influences of site size and electronic configuration on the luminescence bandshapes of matrix-isolated atomic manganese. Although not present in the Mn/RG systems, extrapolations of these influences into larger cubic vacancies, such as the hexavacancy (HV) site, are also provided. The S values listed are the Huang–Rhys factors extracted in the W_p optical function fits conducted in the present study of the $3d^5 4s^2$ configuration and in previous (Refs. 10 and 26) work on the $3d^6 4s^1$ configuration. The abbreviations SOS and CFS indicate resolved spin-orbit splitting and crystal field splitting, respectively.

		Site of isolation		
Electronic config.	Term	SV	TV	HV predicted
$3d^5 4s^2$	$a\,^4P$	SOS	SOS	SOS
		Narrow	Narrow	Narrow
		S=0.0	S=0.0	
	$b\,^4D$	CFS	SOS	SOS
		Narrow	Narrow	Narrow
		S=0.4	S=0.0	
$3d^6 4s^1$	$a\,^4D$		CFS	SOS
		Broad	Narrow	Narrow
		S=6.0	S=0.45	
	$a\,^6D$		CFS	SOS
		Broad	Narrow	Narrow
		S=6.0	S=0.4	

($b\,^4D$/331–332 nm) and unshifted emission ($b\,^4D$/329 nm), free of any discernable phonon structure or splitting, when in the larger red site. These observations point to the roles played by (1) the orbital occupancy of the states involved in a transition and (2) the site occupancy of the metal atom in the lattice. The range of behavior exhibited by matrix-isolated atomic manganese is summarized in Table V. It extends from the narrowest lines exhibited when the orbital occupancy is unchanged in the electronic transition (e.g., $3d^5 4s^2\ b\,^4D_{7/2} \rightarrow 3d^5 4s^2\ a\,^6S_{5/2}$) and the larger (TV) sites are occupied, to the broadest bands which accompany a change in the orbital occupancy (e.g., $3d^6 4s^1\ b\,^4D$ or $a\,^6D \rightarrow 3d^5 4s^2\ a\,^6S$) when the metal atom occupies the smaller SV sites. Intermediate behavior, exhibiting resolved CFS, is found for transitions not involving changes in orbital occupancy but for atoms isolated in small SV sites.

If the site occupancy assignments are correct (that the blue sites correspond to Mn atoms in SVs and the red sites involve TVs) then the critical Mn-RG distances can be identified where CFS is manifested since the sizes of these regular sites of the pure rare gases are known. Thus for the $3d^5 4s^2$ orbital occupancy it is between 3.988 (SV) and 4.676 (TV) Å in MnKr and for the $3d^6 4s^1$ orbital occupancy, CFS has already occurred at 4.676 Å. An interesting trend detected in the blue site $3d^5 4s^2\ b\,^4D_{7/2}$ level is that the CFS increases in the series Ar–Xe. This suggests that the site size plays a more important role in determining the extent of the splitting than the strength of interaction. It would be expected that the increased polarizability of xenon would give rise to the strongest interaction of the three rare gases studied but this is evidently not reflected in the splittings present in the recorded spectra.

A group theoretical analysis[26] of crystal field perturbations of discrete spin-orbit levels indicates that for all J values greater than 3/2, splitting should in theory be exhibited. This raises the interesting possibility of observing CFS of P terms or even the J=5/2 level of the spherically symmetric ^6S (A) ground state of matrix isolated atomic manganese. A very significant observation made in this regard concerns the $3d^5 4s^2\ a\,^4P$ state at approximately 370 nm which in Mn/Xe exhibits a pair of narrow, nonsplit emission features for the J=5/2 and 3/2 spin-orbit levels. As demonstrated elsewhere, group theory predicts that the 5/2 level will split into two levels, but no such splitting is evident in the spectra recorded. With the resolving power of our emission system, the J=5/2 spin-orbit level shows no splitting even though this system has only blue site occupancy in which CFS has been found most pronounced. Thus for terms derived from a common configuration, in this case $3d^5 4s^2$, this behavior would indicate that the spin-orbit levels derived from P terms are less prone to CFS than those derived from D terms. It is well known that crystal fields of cubic symmetry do not induce splitting of P terms so on the basis of the present observations, it would appear that the spatial nature of the term is more important than the degeneracy of the spin-orbit level. More systems need to be studied before a generalization can be provided.

As mentioned earlier, even the symmetric ^6S (A) ground state of atomic manganese should in theory be prone to CFS since it has a J value of 5/2. In an ESR study of ground state Mn atoms isolated in Ne and Ar matrices, Weltner and co-workers[27] identified features in the recorded spectra which indicated zero-field splitting of the S term. The magnitude of the ZFS was $|D| = 0.0071$ cm^{-1} in neon[28] and smaller still in Ar. These values are four orders of magnitude less than the 30 cm^{-1} CFS present on the optical transitions examined in the present study and clearly will not affect the splitting of excitation or emission bands. Nevertheless these magnetic resonance observations do reveal the power of group theoretical methods to analyze the manifestation of competing crystal field and spin-orbit effects in optical spectroscopies.

[1] C. Crepin-Gilbert and A. Tramer, Int. Rev. Phys. Chem. **18**, 485 (1999).
[2] V. E. Bondybey, J. Chem. Phys. **68**, 1308 (1978).
[3] M. J. Pellin, D. M. Gruen, T. Fischer, and T. Foosneas, J. Chem. Phys. **79**, 5871 (1983).
[4] T. A. Cellucci and E. R. Nixon, J. Phys. Chem. **89**, 1991 (1985) and references cited therein to earlier work; In particular, M. T. McKenzie, Ph.D. thesis, University of Pennsylvania, 1983.
[5] H. O. Wiggenhauser, W. Schroeder, and D. M. Kolb, J. Chem. Phys. **88**, 3434 (1988).

[6] S. A. Mitchell, J. Farrell, G. A. Kenney-Wallace, and G. A. Ozin, J. Am. Chem. Soc. **102**, 7702 (1980).

[7] V. A. Bracken, P. Gürtler, and J. G. McCaffrey, J. Chem. Phys. **107**, 5290 (1997).

[8] B. Healy and J. G. McCaffrey, J. Chem. Phys. **110**, 3903 (1999).

[9] M. A. Collier and J. G. McCaffrey, J. Chem. Phys. **119**, 11878 (2003).

[10] M. A. Collier and J. G. McCaffrey, J. Chem. Phys. **122**, 184507 (2005).

[11] M. A. Collier, Ph. D. thesis, National University of Ireland-Maynooth, 2004.

[12] M. A. Ryan, M. Collier, P. de Pujo, C. Crépin, and J. G. McCaffrey, J. Phys. Chem. A **114**, 3011 (2010).

[13] NIST Atomic Spectra Database, website: http://physics.nist.gov/PhysRefData/ASD/ (last accessed December 2009).

[14] J. Shakhsemampour, "Absorption and magnetic circular dichroism of transition metal atoms and small clusters isolated in noble gas matrices," Ph.D. thesis, University of Florida, 1983.

[15] J. C. Rivoal, J. Shakhsemampour, K. K. Zeringue, and M. Vala, Chem. Phys. Lett. **92**, 313 (1982).

[16] M. A. Collier and J. G. McCaffrey, J. Chem. Phys. **122**, 054503 (2005).

[17] C. W. Struck and W. H. Fonger, *Understanding Luminescence Spectra and Efficiency Using W_p and Related Functions* (Springer, Berlin, 1991).

[18] The emission bands in the visible spectral region ($\lambda > 400$ nm) have been analyzed in earlier work, see Ref. 10 for details.

[19] S. M. Younger, J. R. Fuhr, G. A. Martin, and W. L. Wiese, J. Phys. Chem. Ref. Data **7**, 495 (1978).

[20] M. A. Collier, M. A. Ryan, and J. G. McCaffrey, J. Chem. Phys. **123**, 044508 (2005).

[21] P. Cambi, D. Cappelletti, G. Luiti, and F. Pirani, J. Chem. Phys. **95**, 1852 (1991).

[22] J. G. McCaffrey, A. Leung, D. J. Bellert, and W. H. Breckenridge, Chem. Phys. Lett. **302**, 113 (1999).

[23] D. Schwarzhans and D. Zimmermann, Eur. Phys. J. D **22**, 193 (2003) (and references cited therein).

[24] B. diBartolo, *Optical Interactions in Solids* (Wiley, New York, 1968), p. 204.

[25] B. S. Tsukerblat, *Group Theory in Chemistry and Spectroscopy* (Dover, New York, 2006), p. 258.

[26] O. Byrne, M.A. Collier, M.A. Ryan and J.G. McCaffrey, "Crystal field splitting on D↔S transitions of atomic manganese isolated in solid Krypton," J. Low Temp. Physics (in press).

[27] R. J. van Zee, D. A. Garland, and W. Weltner, J. Chem. Phys. **85**, 3237 (1986).

[28] W. Weltner, *Magnetic Atoms and Molecules* (van Nostrand Reinhold, New York, 1983), pp. 28 and 29.